



CHORUS

This is the accepted manuscript made available via CHORUS. The article has been published as:

Magnetic field induced delocalization in hybrid electron-nuclear spin ensembles

Daniela Pagliero, Pablo R. Zangara, Jacob Henshaw, Ashok Ajoy, Rodolfo H. Acosta, Neil Manson, Jeffrey A. Reimer, Alexander Pines, and Carlos A. Meriles

Phys. Rev. B **103**, 064310 — Published 26 February 2021

DOI: [10.1103/PhysRevB.103.064310](https://doi.org/10.1103/PhysRevB.103.064310)

Magnetic-field-induced delocalization in hybrid electron-nuclear spin ensembles

Daniela Pagliero^{1,*}, Pablo R. Zangara^{6,7,*}, Jacob Henshaw¹, Ashok Ajoy³, Rodolfo H. Acosta^{6,7}, Neil Manson⁸, Jeffrey A. Reimer^{4,5}, Alexander Pines^{3,5}, Carlos A. Meriles^{1,2,†}

¹*Department of Physics, CUNY-City College of New York, New York, NY 10031, USA.*

²*CUNY-Graduate Center, New York, NY 10016, USA.*

³*Department of Chemistry, University of California at Berkeley, Berkeley, California 94720, USA.*

⁴*Department of Chemical and Biomolecular Engineering, University of California at Berkeley, Berkeley, California 94720, USA.*

⁵*Materials Science Division Lawrence Berkeley National Laboratory, Berkeley, California 94720, USA.*

⁶*Facultad de Matemática, Astronomía, Física y Computación, Universidad Nacional de Córdoba, Ciudad Universitaria, CP:X5000HUA Córdoba, Argentina.*

⁷*Instituto de Física Enrique Gaviola (IFEG), CONICET, Medina Allende s/n, X5000HUA, Córdoba, Argentina.*

⁸*Laser Physics Centre, Research School of Physics and Engineering, Australian National University, Canberra, A.C.T. 2601, Australia*

*Equally contributing authors. †Corresponding author. E-mail: cmeriles@ccny.cuny.edu

We use field-cycling-assisted dynamic nuclear polarization and continuous radio-frequency (RF) driving over a broad spectral range to demonstrate magnetic-field-dependent activation of nuclear spin transport from strongly-hyperfine-coupled ¹³C sites in diamond. We interpret our observations with the help of a theoretical framework where nuclear spin interactions are mediated by electron spins. In particular, we build on the results from a 4-spin toy model to show how otherwise localized nuclear spins must thermalize as they are brought in contact with a larger ancilla spin network. Further, by probing the system response to a variable driving field amplitude, we witness stark changes in the RF-absorption spectrum, which we interpret as partly due to contributions from heterogeneous multi-spin sets, whose ‘zero-quantum’ transitions become RF active thanks to the hybrid electron-nuclear nature of the system. These findings could prove relevant in applications to dynamic nuclear polarization, spin-based quantum information processing, and nanoscale sensing.

Keywords: Nuclear spin diffusion | Dynamic nuclear polarization | Nitrogen-vacancy centers | Thermalization

I. INTRODUCTION

Nuclear spin-lattice relaxation in insulators is governed by interactions with paramagnetic centers within the material host, a notion first introduced by Bloembergen more than half a century ago¹. Since these interactions strongly depend on the distance to the paramagnetic defect, the dynamics of nuclear spin thermalization emerges from an interplay between local relaxation rates and inter-nuclear couplings. In the simplest picture, nuclear spins sufficiently removed from the paramagnetic center converge jointly to a common temperature via spin diffusion, the energy-conserving process where a nuclear spin ‘flips’ at the expense of a ‘flop’ by a neighbor². By contrast, strong magnetic field gradients near the defect — and the corresponding energy shifts they produce — disrupt spin exchange, prompting a description in terms of thermally disconnected regions of space — ‘bulk’ and ‘local’ spins — separated by a ‘diffusion barrier’. The latter amounts to an imaginary surface where electron-nuclear and inter-nuclear spin couplings become comparable³.

While the ideas above have undeniably proven valuable, they implicitly rest on a simplified scenario where the electronic spin bath is sufficiently dilute, i.e., where couplings between electronic spins are negligible. The impact these interactions can have in rendering the diffusion barrier

permeable was first highlighted by Wolfe and collaborators in experiments with rare-earth-doped garnets at various concentrations^{4,5}. More recently, the widespread use of dynamic nuclear polarization (DNP) methods have brought new attention to these early results as there is an inextricable connection between polarization flow and spin thermalization⁶⁻⁹. For example, experiments at low temperatures and high magnetic fields in radical-hosting organic matrices have exposed the combined impact of continuous microwave (MW) excitation and electron spectral diffusion on observed DNP ‘spectra’ (i.e., the observed nuclear magnetic resonance (NMR) signal as a function of the applied MW frequency)^{10,11}. Further, electron-driven spin diffusion was introduced recently as a mechanism for nuclear polarization transfer in the proximity of paramagnetic defects¹². Along related lines, DNP of carbon spins in diamond was exploited to reveal electron-spin-mediated nuclear spin diffusion exceeding the value expected for naturally abundant ¹³C spins by nearly two orders of magnitude¹³.

Beyond applications to NMR signal enhancement, the interplay between diffusion and localization at the core of DNP can also be seen as an opportunity to investigate fundamental problems, most notably the competition between disorder and long-range interactions found in the out-of-equilibrium dynamics of driven open systems^{14,15}.

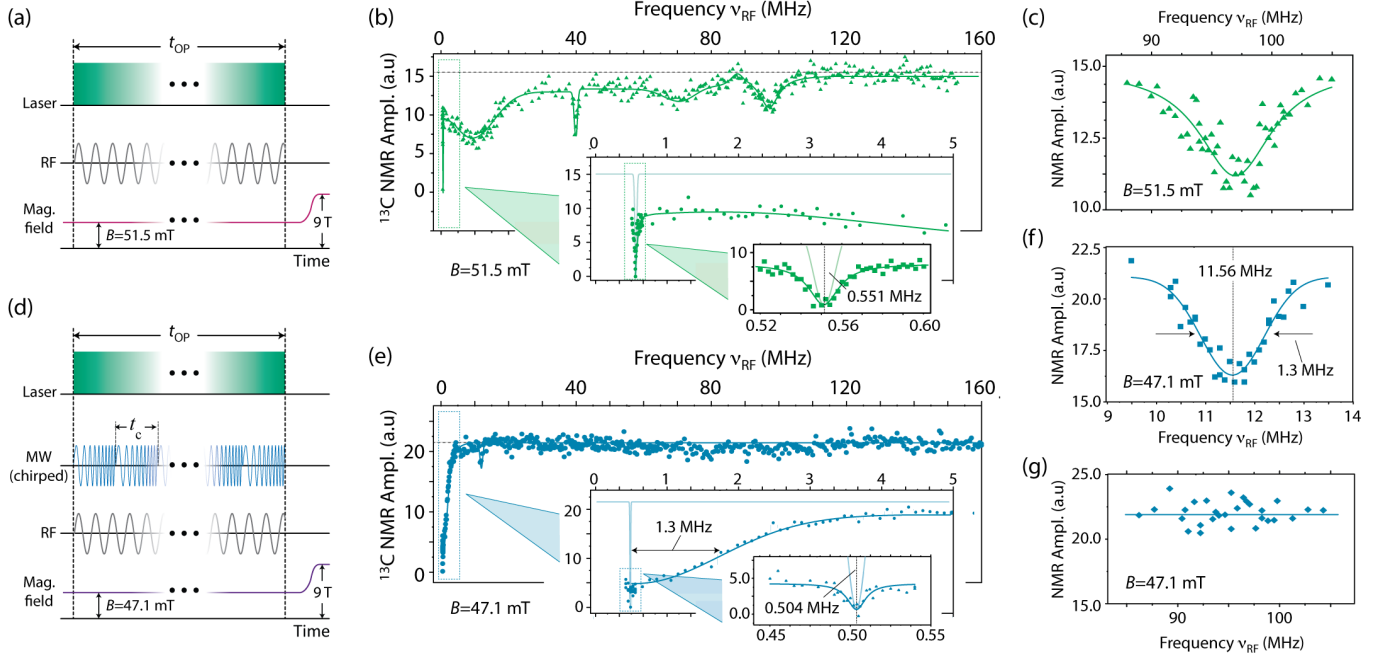


Figure 1 | The role of P1 centers. (a) Static matching field (SMF) protocol. (b) ^{13}C NMR signal amplitude as a function of ν_{RF} ; the external magnetic field is $B^{(+)} = 51.5$ mT. (c) Zoomed SMF response around ~ 97 MHz. (d) Dynamic nuclear polarization via microwave sweeps (MWS). (e) Same as in (b) but using the MWS protocol to induce nuclear polarization; the external magnetic field is $B = 47.1$ mT. (f-g) Zoomed ^{13}C response using the MWS protocol. Unlike (b), we see no high-frequency dips. In all experiments, $t_{\text{OP}} = 5$ s, the total number of repeats per point is 8, the driving field amplitude is $\Omega_{\text{RF}} = 4$ kHz, and the laser power is 1 W; solid traces are guides to the eye. In (d) through (g), the MW power is 300 mW, the sweep range is 25.2 MHz centered around the NV $|0\rangle \leftrightarrow |-1\rangle$ transition, the sweep rate is 15 MHz ms^{-1} corresponding to a total of 8333 sweeps during t_{OP} .

Indeed, disorder and quantum interference can stymie thermalization, often leading to regimes of sub-diffusive dynamics or suppressed transport, a broad, fundamental phenomenon found in systems ranging from electrons in a crystal with disorder¹⁶ to optical waves in a photonic structure¹⁷. Despite their differences, they all share similarities in that their Hamiltonians can often be mapped to those governing the dynamics of electron/nuclear spin sets in a solid.

Here, we resort to nuclear spins in diamond to demonstrate control over the localization/delocalization dynamics of hyperfine-coupled carbons upon variation of the applied magnetic field. We formally capture our observations by considering a model electron-nuclear spin chain featuring magnetic-field-dependent spin transport. Further, the dynamics at play can be cast in terms of distinct dynamic regimes that can be accessed by tuning the magnetic field strength and (effective) paramagnetic content. The spin state hybridization emerging from the intimate connection between electron and nuclear spins gives rise to otherwise forbidden low-frequency transitions, whose presence underlies the system's singular spectral response to RF excitation of variable amplitude.

II. RESULTS

A. Probing nuclear spin polarization transport at variable magnetic field

In our experiments, we dynamically polarize and probe

^{13}C spins in a $[100]$ diamond crystal ($3 \times 3 \times 0.3$ mm³) grown in a high-pressure/high-temperature chamber (HPHT). The system is engineered to host a large (~ 10 ppm) concentration of nitrogen-vacancy (NV) centers, spin-1 paramagnetic defects that polarize efficiently under green illumination. Coexisting with the NVs is a more abundant group of P1 centers (~ 50 ppm), spin-1/2 defects formed by substitutional nitrogen atoms. We tune the externally applied magnetic field B in and out the ‘energy matching’ range centered at B_m (~ 51.8 mT for our present experimental conditions), where the Zeeman splitting of the P1 spins coincides with the frequency gap between the $|0\rangle$ and $|-1\rangle$ states of the NVs. Following electron and nuclear spin manipulation, we monitor the bulk ^{13}C polarization via high-field NMR upon shuttling the sample into the bore of a 9 T magnet (additional experimental details can be found in Ref. (18)).

Fig. 1a shows a typical experimental protocol: We continuously illuminate the sample with a green laser (1 W at 532 nm) during a time interval $t_{\text{OP}} = 5$ s while simultaneously applying continuous radio-frequency (RF) excitation; here we set the field at 51.5 mT, slightly below B_m , where nuclear spins polarize positively as they provide the energy necessary to enable an NV-P1 ‘flip-flop’¹⁸. Figs. 1b and 1c show the resulting spectrum obtained as we measure the bulk ^{13}C NMR signal for different RF frequencies ν_{RF} within the range 0.5-160 MHz. Besides the dip at 551 kHz — corresponding to the Larmor frequency of bulk ^{13}C at $B = 51.5$ mT — we find several RF absorption bands, indicative of polarization transport from electron spins

to bulk carbons via select groups of strongly hyperfine-coupled nuclei¹³.

As an alternative to nuclear/electron spin cross-relaxation, one can dynamically polarize carbons via the use of chirped micro-wave (MW) pulses, consecutively applied during $t_{OP}^{19,20}$ (Fig. 1d). Unlike the case above, nuclear spin polarization stems this time from Landau-Zener dynamics near level anti-crossings induced in the rotating frame as the MW sweeps the NV transitions²⁰ (specifically, the $|0\rangle \leftrightarrow |-1\rangle$ transition in the present case). Upon simultaneous RF excitation at variable frequencies, the spectrum that emerges indicates the polarization transport process is fundamentally distinct. This is shown in Figs. 1e through 1g, where we set the magnetic field to 47.1 mT, a shift of only ~ 4 mT from the experiments in Figs. 1a and 1b (yet sufficiently strong to quench cross-polarization-driven DNP¹⁸). In particular, we find that the RF impact is mostly limited to a ~ 1.3 MHz band adjacent to the ¹³C Larmor frequency (~ 0.5 MHz at 47 mT, insert in Fig. 1e). The differences are most striking near 40 MHz and 97 MHz where the dips observed at 51 mT (Figs. 1b and 1c) virtually vanish (Figs. 1e and 1g). Similarly, the small RF dip at ~ 11 MHz (Figs. 1e and 1f) amounts to only a little fraction of the broad absorption band centered at that frequency under field matching (Fig. 1b).

Before attempting to set these observations on a formal footing, we note that the generation and transport of nuclear spin polarization are two distinct physical processes: While the former provides the basis to understanding how order is transferred from electron to nuclear spins, our experiments allow us to investigate the latter, namely how strongly-hyperfine-coupled spins pass on polarization to ‘bulk’ nuclei (i.e., carbons whose hyperfine couplings are weaker than their mutual dipolar interactions). This question is particularly intriguing in diamond because ¹³C spins are relatively dilute ($\sim 1\%$) thus yielding weak dipolar couplings (~ 100 Hz), orders of magnitude smaller than typical hyperfine interactions (often in the ~ 1 -10 MHz range and reaching up to ~ 130 MHz for first shell nuclei). Note that generation and transport are both necessary ingredients in the observation of DNP, implying that the absolute NMR signal amplitude per se — slightly different if cross-polarization or chirped MW is used to produce nuclear polarization, see Fig. 1 — has little intrinsic meaning. By contrast, we show below how the RF absorption spectra we measure allow us to gain a deeper understanding of the dynamics at play.

B. Modeling transport via electron/nuclear spin sets

In the language of magnetic resonance, spin transport in DNP has been traditionally cast in terms of a ‘spin-diffusion barrier’, i.e., a virtual boundary around individual paramagnetic defects separating bulk spins from a ‘frozen’ nuclear core whose polarization cannot diffuse (simply because nuclear ‘flip-flops’ are energetically quenched). Avoiding such a scenario would require, in general, that polarization be generated via direct transfer from the defect to weakly coupled nuclei (featuring hyperfine constants of order ~ 100 Hz or less in the present case), a condition clearly inconsistent with the observations in Fig. 1 (both within or

outside the NV/P1 field matching range). Further, the stark differences between the RF-absorption spectra observed in either case indicate that the very notion of a diffusion barrier as an inherent sample feature must be re-examined.

Although disorder in the crystal creates virtually countless combinations of interacting nuclear and electron spins, a concise description of nuclear spin transport demands the simplest possible spin set. On the other hand, the energy-conserving nature of this process imposes a minimum conceptual threshold: For instance, 3-spin sets — comprising, e.g., two electron spins and a carbon — provide an intuitive platform to describe polarization transfer from electrons to nuclei — the so-called ‘cross effect’ — but is clearly inadequate to describe polarization transport to bulk nuclei. Similar considerations apply to sets comprising two carbons and an electron spin because, under our experimental conditions, the energy change emerging from polarization hopping from one nuclear spin to the other is much smaller than the electron spin Zeeman energy at the applied magnetic field (~ 1.44 GHz), thus inhibiting electron/nuclear polarization transfer (see Section I in Ref. [21] for a formal discussion).

The above difficulties, however, can be circumvented with the toy model in Fig. 2a, a chain comprising an interacting pair of NV–P1 electron spins, each of them coupled to a neighboring carbon via hyperfine tensors of magnitude $\|A_j\|$ with $j = 1, 2$; for illustration purposes, we focus on the ‘hyperfine-dominated’ regime $\|A_1\| \sim \|A_2\| > J_d > \omega_1$, where J_d is the NV–P1 dipolar coupling constant, and ω_1 is the nuclear Larmor frequency. Intuitively, this system supports spin transport because changes in the nuclear and electronic spin energies compensate each other when the magnetic field takes on select transport-enabling values slightly shifted from B_m , namely $B_m^{(\varepsilon)} = B_m + \delta B^{(\varepsilon)}$, with $\varepsilon = \alpha, \beta$, each corresponding to alternative sets of degenerate spin configurations of the chain²¹.

In the absence of hyperfine couplings to the host nitrogen nucleus of either paramagnetic defect (a condition assumed here for simplicity), and using \mathbf{I}_1 (\mathbf{I}_2) to denote the vector spin operator of the nuclear spin coupled to the NV (P1), one can show that ¹³C spins in the chain are governed by the effective Hamiltonian²¹

$$H_{\text{eff}} = \delta_{\text{eff}} I_1^z - \delta_{\text{eff}} I_2^z + J_{\text{eff}} (I_1^+ I_2^- + I_1^- I_2^+), \quad (1)$$

valid near either of the matching points. In the above expression, $\delta_{\text{eff}} = 2\gamma_e \left| B - B_m^{(\alpha, \beta)} \right|$ is the effective nuclear spin frequency offset relative to the matching field $B_m^{(\alpha, \beta)}$, γ_e is the electron spin gyromagnetic ratio, and we assume all spin operators are unit-less (i.e., $\hbar = 1$). Further, the effective coupling between nuclear spins is given by $J_{\text{eff}} = -\omega_1 J_d (A_2^{zx} / \Delta_2^z) \sin(\frac{\theta}{2})$, where $\Delta_2^z = (A_2^{zz})^2 + (A_2^{zx})^2$, $\tan(\theta) \approx A_1^{zx} / A_1^{zz}$, and A_j^{zz} (A_j^{zx}) denotes the secular (pseudo-secular) hyperfine coupling constant for nuclear spin $j = 1, 2$.

Eq. (1) is a nuclear-spin-only Hamiltonian where

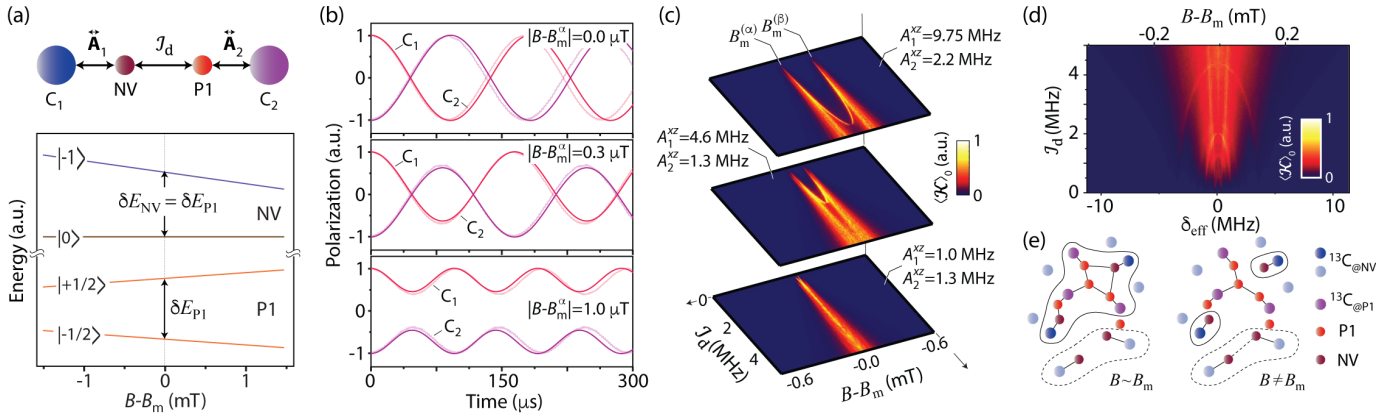


Figure 2 | Magnetic-field-dependent spin transport. (a) Model spin chain (top) and schematic NV–P1 energy diagram; at the matching field B_m , the Zeeman splitting of the P1 coincides with the energy separation of the NV $|0\rangle \leftrightarrow |-1\rangle$ transition. (b) Inter-carbon polarization transfer for the chain in (a). The solid (faint) traces in each plot show the calculated evolution under the effective (exact) Hamiltonian assuming $J_d = 0.7$ MHz, $A_1^{zz} = 13$ MHz, $A_2^{zz} = 4$ MHz, and $A_j^{zz} = A_j^{zx}$ for $j = 1, 2$. (c) Nuclear spin current amplitude $\langle \mathcal{K} \rangle_0$ for the chain in (a) as a function of B and J_d for different hyperfine couplings. (d) Same as in (c) but after a weighted average over various configurations of hyperfine couplings (see Ref. 21). (e) Schematics of spin dynamics. (Left) When $B \sim B_m$, ^{13}C spins strongly coupled to NVs (dark blue and dark red circles, respectively) communicate with each other via networks formed by ^{13}C spins hyperfine-coupled to P1s (purple and light red circles, respectively). (Right) Away from the energy matching range, strongly coupled carbons become localized. Weaker inter-NV interactions can mediate the transport of nuclear polarization seeded in carbons featuring intermediate or weak hyperfine couplings (light blue circles).

paramagnetic interactions manifest in the form of field-dependent shifts and effective couplings largely exceeding the intrinsic ^{13}C - ^{13}C dipolar couplings. For example, for the present 50 ppm nitrogen concentration, we have $J_d \sim 3$ MHz and thus $J_{\text{eff}} \sim 30$ kHz for $A_j^{zz} \sim A_j^{zx} \sim 10$ MHz, $j = 1, 2$. A numerical example demonstrating good agreement between the exact and effective nuclear spin evolution is presented in Fig. 2b for three different magnetic fields. It is worth highlighting the amplified sensitivity to field detuning $|B - B_m^{(\alpha, \beta)}|$, impacting the offset terms in Eq. (1) via the electronic (not the nuclear) spin gyromagnetic ratio. We stress that the 4-spin model described above must be seen as the simplest set — among many others — compatible with an effective theory of nuclear magnetization transport as seen in our experiments. More general scenarios are discussed below.

To more generally capture the nuclear spin dynamics prompted by NV–P1 couplings, we resort to the nuclear spin current operator $\mathcal{K} = (1/2i)(I_1^- I_2^+ - I_1^+ I_2^-)$, whose mean value — in general, a function of time t — can be expressed as $\langle \mathcal{K} \rangle(t) = \langle \mathcal{K} \rangle_0 f(t)$, where $f(t)$ is a periodic function of unit amplitude²¹. Using $\langle \mathcal{K} \rangle_0$ as a measure of delocalization²², we benchmark nuclear spin transport in Fig. 2c for different combinations of hyperfine couplings as a function of B and J_d . We find non-zero transport within a confined region of the parameter space, with local maxima at fields $B_m^{\alpha, \beta}$, discernible at weak inter-electronic couplings. Since these express the number of configurations compatible with nuclear spin transport, we anticipate additional matching fields should be present for more complex spin systems.

Our ability to externally activate transport is already implicit in the effective Hamiltonian in Eq. (1), which, upon

the extension to a larger number of spins, can be mapped into the standard Anderson localization problem by means of the Wigner-Jordan transformation. Conceptually, the dynamics in the present spin system can be cast in terms of an interplay between ‘disorder’ — here expressed as site-selective nuclear Zeeman frequencies — and the amplitude of ^{13}C - ^{13}C ‘flip-flop’ couplings J_{eff} — also referred to as the ‘hopping’ term in charge transport studies. Sufficiently close to the matching condition, $\delta_{\text{eff}} \lesssim J_{\text{eff}}$ and the nuclear spins can flip-flop resonantly. On the other hand, a moderate detuning of the magnetic field yields $\delta_{\text{eff}} \gg J_{\text{eff}}$, putting the system back into a strongly localized dynamical phase. This is summarized in Fig. 2d where we compute a weighted average that takes into account the known set of carbon hyperfine couplings with the NV and P1 centers^{21,23-26}, and find non-zero current in the region where $J_{\text{eff}} \gtrsim \delta_{\text{eff}}$. We warn this latter condition must be understood in a distributional sense, i.e., for a given concentration of paramagnetic centers represented by J_d , there is a magnetic field range where spin diffusion channels become available to the most likely spin arrays in the crystal.

It is inevitable to draw a comparison between the distinct spin localization regimes we witness here and the dynamic phase diagram for charge carriers in a solid with disorder, as first introduced by Kimball²⁷. Unfortunately, our experiments do not allow us to gradually transition from one regime to the other, with the consequence that we cannot presently probe criticality at the boundaries as seen in other experiments²⁸⁻³¹. Assuming the proper experimental tools can be put in place, it will be interesting to devote additional work to characterize this system’s response in intermediate regimes.

C. Beyond the 4-spin model

Since the use of chirped MW pulses does produce

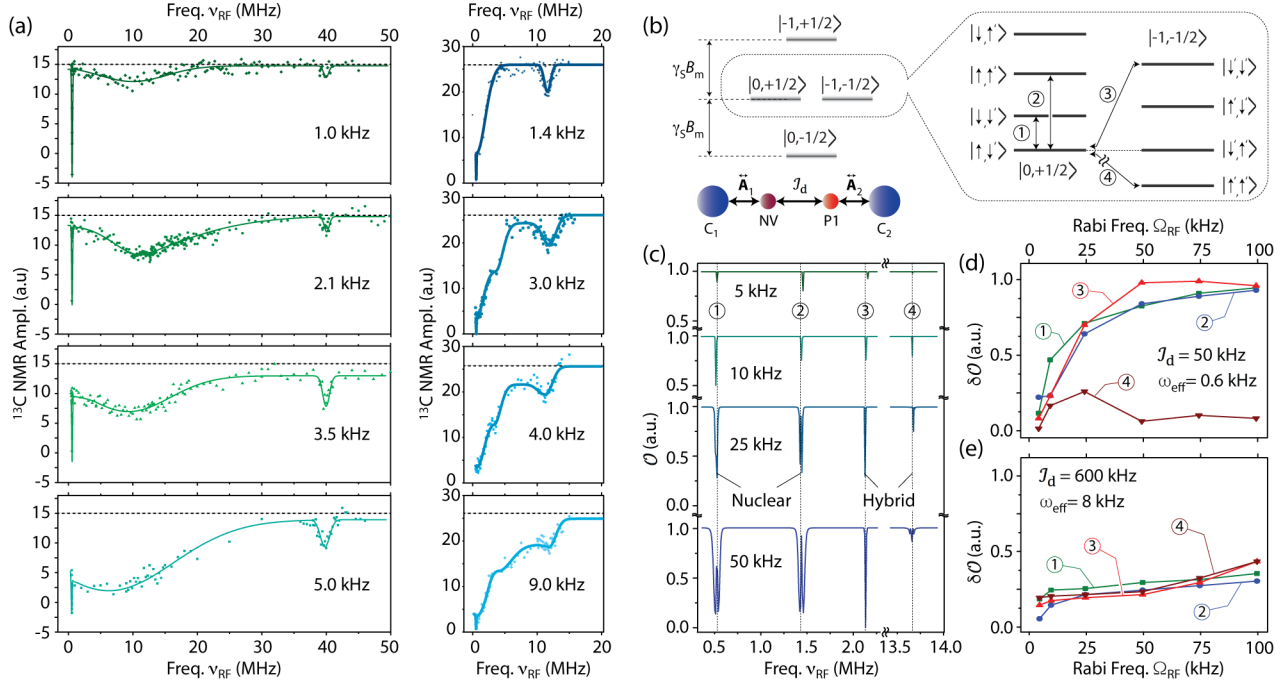


Figure 3 | Dependence with RF power. (a) ^{13}C NMR signal amplitude as a function of the excitation frequency ν_{RF} using the DNP protocols in Figs. 1a and 1d (respectively, left and right panels) for various RF amplitudes (bottom right in each panel). Horizontal dashed lines indicate the ^{13}C NMR amplitude in the absence of RF excitation and solid traces are guides to the eye. (b) Schematic energy diagram for the electron-nuclear spin chain in the cartoon assuming the matching field $B = B_m^\alpha$. States are denoted using projection numbers for the electronic spin and up/down arrows for nuclear spins with primes indicating a dominating hyperfine field. Numbers illustrate some nuclear and electron-nuclear spin transitions; energy separations are not to scale. (c) Spectral overlap \mathcal{O} as a function of ν_{RF} for different Rabi amplitudes Ω_{RF} in the case of a spin chain with couplings $J_d = 30$ kHz, $A_1^{xz} = 9$ MHz, $A_2^{xz} = 2.5$ MHz, and $A_j^{zz} = A_j^{zx}$ for $j = 1, 2$. (d) Spectral overlap change $\delta\mathcal{O}$ at select frequencies (bottom right) as a function of Ω_{RF} for the spin chain in (c). (e) Same as in (d) but for a spin chain with couplings $J_d = 800$ kHz, $A_1^{xz} = 9$ MHz, $A_2^{xz} = 2.5$ MHz, and $A_j^{zz} = A_j^{zx}$ for $j = 1, 2$.

observable ^{13}C signal, it is clear that spin transport outside the above field range is also granted, though the observations in Fig. 1 indicate the enabling channels are different. Direct MW-assisted polarization of bulk nuclei can be ruled out immediately because the results in Fig. 1e show ^{13}C spins with couplings as large as ~ 1 MHz — approximately 4 orders of magnitude greater than homonuclear interactions — do play a key role in the transport. Further, a detailed analysis of chirp-pulse-driven DNP in diamond²⁰ shows that polarization transfer — governed by Landau-Zener dynamics at level anti-crossings in the rotating frame — is highly efficient for carbons featuring hyperfine couplings greater than ~ 1 MHz, but decays sharply for more-weakly interacting nuclei. Correspondingly, the sharp differences between the RF absorption spectra in Fig. 1 point to a distinct polarization transport mechanism where strongly coupled carbons, though polarized, communicate with the rest less efficiently.

While the model spin chain above fails to produce nuclear polarization transport away from the matching field range, we hypothesize that other, larger spin clusters featuring source and target ^{13}C -NV dimers can still maintain transport through higher-order channels, though a formal description becomes increasingly complex^{21,32}. One interesting example is the 5-spin chain $^{13}\text{C}_1\text{-NV}_1\text{-P1-NV}_2\text{-}^{13}\text{C}_2$ whose states $|\downarrow, 0, +1/2, -1, \uparrow\rangle$ and $|\uparrow, -1, +1/2, 0, \downarrow\rangle$

become degenerate when the inter-electronic dipolar coupling and hyperfine energies are suitably matched. Conversion of one into the other occurs via the virtual intermediate state $|\uparrow, -1, -1/2, -1, \uparrow\rangle$ at a rate of order $J'_{\text{eff}} \sim \sin^2\left(\frac{\theta}{2}\right) J_d^2 / (|\gamma_e| \delta B_m)$, where δB_m is the shift relative to the matching field. Note that because of the compensation between dipolar and hyperfine energies, large disparities between Δ_1 and Δ_2 (present only when at least one of the hyperfine couplings is large) cannot be easily accommodated by a reconfiguration of the electronic dipoles ($J_d \lesssim 3$ MHz at the present paramagnetic center concentration). The result is that transport processes involving carbons strongly coupled to NVs get suppressed, in qualitative agreement with our observations. At the same time, polarization exchange remains efficient for moderately coupled nuclei: For example, for $\Delta_1 \sim \Delta_2 \sim 1$ MHz and $|\Delta_1 - \Delta_2| \sim 100$ kHz, we obtain $J'_{\text{eff}} \sim 2$ kHz (we assume $J_d \sim 1$ MHz and use $|\gamma_e| \delta B_m \sim 120$ MHz, consistent with the conditions in Fig. 1e).

It is worth emphasizing that the increased degrees of freedom in the 5-spin set presented above are key to enabling inter-carbon spin transport, as a lengthy analysis of simpler chains shows; in particular, we find that no polarization exchange (other than the trivial case involving nuclei with

identical hyperfine couplings) can take place away from the matching field if one or two electrons in the 5-spin chain are removed; the same is true if one of the NVs is replaced by a P1 (because the degeneracy between states involving different nuclear spin projections cannot be regained). Naturally, it is reasonable to expect transport contributions from other, more complex multi-spin arrays. Additional modeling and experiments (e.g., in the form of RF absorption spectra at fields farther removed from B_m) will therefore be necessary to gain a fuller understanding.

In spite of the present limitations, we can tentatively interpret the markedly different frequency responses in Figs. 1b and 1e as the manifestation of two complementary spin transport regimes, one relying on field-enabled matching between NV and P1 resonances, the other emerging from P1-mediated interactions between NV-coupled carbons. A schematic is presented in Fig. 2e, where we generalize to more complex spin sets: ^{13}C spins strongly coupled to NVs — otherwise thermalizing with the rest through the help of P1-based networks — become localized when the magnetic field departs sufficiently from B_m . In this regime, dipolar P1-mediated interactions between NVs can help transport the polarization induced by chirped MW pulses in the (more-weakly-coupled) carbons in their vicinity. In particular, we hypothesize this latter mechanism underlies the disappearance or reduction of all dips above ~ 1 MHz in the RF absorption spectrum at 47.1 mT (Figs. 1e and 1f). Note that although chains involving only P1s — i.e., with no NVs — remain efficient spin exchange routes away from B_m ¹³, such transport channels are not observable here because MW pulses selectively seed polarization in nuclei coupled to NVs, not P1s (i.e., an all-P1 chain can impact the NMR signal only in the less-likely scenario where the seed carbon is simultaneously coupled to an NV and a P1).

D. Understanding the impact of RF on multi-spin electron/nuclear networks

Additional information on the dynamics at play can be obtained through the experiments in Fig. 3, where we measure the DNP response under the protocols of Figs. 1a and 1d using RF excitation of variable power. Besides the anticipated gradual growth of the absorption dips, we observe an overall spectral broadening, greatly exceeding that expected from increased RF power alone. This behavior is clearest in the range 5–15 MHz and near 40 MHz (Fig. 3a), where all absorption dips grow to encompass several MHz even when the RF Rabi field Ω_{RF} never exceeds 10 kHz.

To interpret these observations, we resort one more time to the electron–nuclear spin chain in Fig. 2a and model the system dynamics in the presence of a driving RF field with no approximations^{21,33}. Since optical initialization of the NV into $|0\rangle$ imposes a time dependence on the mean magnetization $\langle I_j^z \rangle$, $j = 1, 2$ of either nuclear spin in the chain²¹, we gauge the impact of the drive at frequency ν_{RF} and amplitude Ω_{RF} via the overlap function $\mathcal{O}(\nu_{\text{RF}}, \Omega_{\text{RF}}) = \zeta \left| \int d\omega \langle I_1^z \rangle_\omega \langle I_2^z \rangle_\omega^* \right|$, where $\langle I_j^z \rangle_\omega = \int dt e^{i\omega t} \langle I_j^z \rangle(t, \nu_{\text{RF}}, \Omega_{\text{RF}})$ is the Fourier transform of the

magnetization in carbon $j = 1, 2$, and ζ is a normalization constant calculated as the inverse of the spectral overlap $\left| \int d\omega \langle I_1^z \rangle_\omega \langle I_2^z \rangle_\omega^* \right|_0$, where the subscript denotes the absence of a drive (i.e., $\Omega_{\text{RF}} = 0$). Maximum by default, $\mathcal{O}(\nu_{\text{RF}}, \Omega_{\text{RF}})$ decreases when ν_{RF} is made resonant with one of the possible nuclear/electron spin transitions in the chain (see schematic energy diagram in Fig. 3b), thus allowing one to quantify the RF-induced disruption of transport through the appearance of ‘dips’ at select frequencies²¹.

For illustration purposes, Fig. 3c shows the calculated response of a 4-spin chain with inter-electronic coupling $J_d = 30$ kHz assuming one of the transport-enabling conditions, $B = B_m^{(a)}$. RF-absorption at select frequencies perturbs inter-nuclear transport hence leading to a reduction of the spectral overlap $\mathcal{O}(\nu_{\text{RF}}, \Omega_{\text{RF}})$. A detailed inspection shows that some of these resonances can be associated to ‘zero-quantum’ (i.e., intra-band) transition frequencies in the electron bath. Normally forbidden, these transitions are activated here due to the hybrid, nuclear–electron spin nature of the chain (e.g., transitions (3) and (4) in Fig. 3b, see also Ref. 21). The separation between consecutive dips is determined by the inter-electron and hyperfine couplings, thus leading to complex spectral responses spanning several MHz.

Fig. 3d shows the calculated spectral overlap change $\delta\mathcal{O} \equiv \mathcal{O}(\Omega_{\text{RF}}, \nu_{\text{RF}}) - 1$ as a function of Ω_{RF} at select excitation frequencies ν_{RF} : Interestingly, we find that all dips — both nuclear and hybrid — grow at comparable rates, a counter-intuitive response given the presumably hindered nature of the zero-quantum transitions²¹. On the other hand, the transport of nuclear spin polarization — faster for chains featuring greater J_d — is more difficult to disrupt if $\Omega_{\text{RF}} \lesssim J_{\text{eff}}, J'_{\text{eff}}$, thus leading to slower growth rates for more strongly coupled chains (Fig. 3e). Correspondingly, the response expected for spins in a crystal (vastly more complex than our toy model) is one where RF excitation of increasing amplitude gradually induces new dips through the perturbation of faster polarization transport channels. The result is a progressively broader-looking absorption spectrum, in qualitative agreement with our observations. Note that this picture also applies to the case where chirped MW excitation is simultaneously present (right panels in Fig. 3a), because the time interval (~ 2 ms) separating consecutive sweeps is typically longer than the inverse effective coupling, $(J'_{\text{eff}})^{-1}$, thus ensuring the MW-induced disruption on polarization transport is minor.

III. CONCLUSIONS

In summary, by monitoring changes in the DNP signal of ^{13}C spins in diamond in the presence of an RF drive we show that hyperfine-coupled nuclei are central to the transport of spin polarization in the crystal. Further, different transport channels (involving nuclei featuring stronger or weaker hyperfine interactions) activate or not depending on the applied magnetic field. We conclude from this finding that the widespread notion of a spin-diffusion barrier intrinsic to the system under investigation is inaccurate, namely,

strongly-hyperfine-coupled nuclei localize or delocalize depending on the ‘connectivity’ of interacting paramagnetic centers — itself a function of the defect concentration — here effectively controlled via the applied magnetic field.

Upon varying the amplitude of the drive, we witness gradual changes in the RF absorption spectrum — crudely manifesting as an overall broadening — which we analyze by considering the impact of continuous excitation on the dynamics of electron/nuclear spin chains. We find the RF drive disrupts nuclear spin transport through the activation of single- and many-spin transitions, the latter class involving both electron and nuclear spin flips. Our calculations show that systems featuring stronger inter-electronic couplings are less sensitive to RF excitation, indicating that the observed spectral changes stem from an inhomogeneous response where various spin sets — initially unaffected by weaker drives — gradually stop transporting nuclear polarization to the bulk as the RF amplitude grows. This view is consistent with the intuitive idea of multiple transport channels simultaneously coexisting in a disordered system.

Despite its present limitations, our model suggests we should view these many-spin sets as a single whole, where nominally forbidden ‘hybrid’ excitations applied locally propagate spectrally to impact groups of spins not directly

addressed. Therefore, besides the fundamental aspects, an intriguing practical question is whether, even in the absence of optical pumping, Overhauser- or Solid-Effect-like DNP — normally relying on strong MW excitation — can be attained more simply via low-frequency (i.e., RF) manipulation of the electron spins using nuclei as local handles. More generally, these results could prove useful in quantum applications relying on spin platforms, for example, to transport information between remote nuclear qubits or to develop enhanced nanoscale sensing protocols.

IV. ACKNOWLEDGEMENTS

D.P., J.H., and C.A.M. acknowledge support from the National Science Foundation through grant NSF-1903839, and from Research Corporation for Science Advancement through a FRED Award; they also acknowledge access to the facilities and research infrastructure of the NSF CREST IDEALS, grant number NSF-HRD-1547830. J.H. acknowledges support from CREST-PRF NSF-HRD 1827037. P.R.Z. and R.H.A. acknowledge financial support from CONICET (PIP-111122013010074 6CO), SeCyT-UNC (33620180100154CB) and ANPCYT (PICT-2014-1295).

¹ N. Bloembergen, “On the interaction of nuclear spins in a crystalline lattice”, *Physica* **25**, 386 (1949).

² G.R. Khutsishvili, “Spin diffusion and magnetic relaxation of nuclei”, *Sov. Phys. JETP* **15**, 909 (1962).

³ W.E Blumberg, “Nuclear spin-lattice relaxation caused by paramagnetic impurities”, *Phys. Rev.* **119**, 79 (1960).

⁴ J.P. Wolfe, “Direct observation of a nuclear spin diffusion barrier”, *Phys. Rev. Lett.* **31**, 907 (1973).

⁵ A.D.A. Hansen, J.P. Wolfe, “Measurement of the nuclear spin diffusion barrier around Eu²⁺ ions in CaF₂”, *Phys. Lett. A* **66**, 320 (1978).

⁶ A.A. Smith, B. Corzilius, A.B. Barnes, T. Maly, R.G. Griffin, “Solid effect dynamic nuclear polarization and polarization pathways”, *J. Chem. Phys.* **136** 015101 (2012).

⁷ K.O. Tan, M. Mardini, C. Yang, J.H. Ardenkjær-Larsen, R.G. Griffin, “Three-spin solid effect and the spin diffusion barrier in amorphous solids”, *Sci. Adv.* **5**, eaax2743 (2019).

⁸ C. Ramanathan, “Dynamic nuclear polarization and spin diffusion in nonconducting solids”, *Appl. Magn. Reson.* **34**, 409 (2008).

⁹ A.E. Dementyev, D.G. Cory, C. Ramanathan, “Rapid diffusion of dipolar order enhances dynamic nuclear polarization”, *Phys. Rev. B* **77**, 024413 (2008).

¹⁰ Y. Hovav, D. Shimon, I. Kaminker, A. Feintuch, D. Goldfarb, S. Vega, “Effects of the electron polarization on dynamic nuclear polarization in solids”, *Phys. Chem. Chem. Phys.* **17**, 6053 (2015).

¹¹ A. Leavesley, D. Shimon, T.A. Siaw, A. Feintuch, D. Goldfarb, S. Vega, I. Kaminkera, S. Han, “Effect of electron spectral diffusion on static dynamic nuclear polarization at 7 Tesla”, *Phys. Chem. Chem. Phys.* **19**, 3596 (2017).

¹² J.J. Wittmann, M. Eckardt, W. Harneit, B. Corzilius, “Electron-driven spin diffusion supports crossing the diffusion barrier in MAS DNP”, *Phys. Chem. Chem. Phys.* **20**, 11418 (2018).

¹³ D. Pagliero, P. Zangara, J. Henshaw, A. Ajoy, R.H. Acosta, J.A. Reimer, A. Pines, C.A. Meriles, “Optically pumped spin polarization as a probe of many-body thermalization”, *Science Adv.* **6**, eaaz6986 (2020).

¹⁴ A. De Luca, A. Rosso, “Dynamic nuclear polarization and the paradox of quantum thermalization”, *Phys. Rev. Lett.* **115**, 080401 (2015).

¹⁵ A De Luca, I. Rodríguez-Arias, M. Müller, A. Rosso, “Thermalization and many-body localization in systems under dynamic nuclear polarization”, *Phys. Rev. B* **94**, 014203 (2016).

¹⁶ E. Abrahams, *50 years of Anderson Localization*, World Scientific, 2010.

¹⁷ T. Schwartz, G. Bartal, S. Fishman, M. Segev, “Transport and Anderson localization in disordered two-dimensional photonic lattices”, *Nature* **446**, 52 (2007).

¹⁸ D. Pagliero, K.R. Koteswara Rao, P.R. Zangara, S. Dhomkar, H.H. Wong, A. Abril, N. Aslam, A. Parker, J. King, C.E. Avalos, A. Ajoy, J. Wrachtrup, A. Pines, C.A. Meriles, “Multispin-assisted optical pumping of bulk ¹³C nuclear spin polarization in diamond”, *Phys. Rev. B* **97**, 024422 (2018).

¹⁹ A. Ajoy, K. Liu, R. Nazaryan, X. Lv, P.R. Zangara, B. Safvati, G. Wang, D. Arnold, G. Li, A. Lin, P. Raghavan, E. Druga, S. Dhomkar, D. Pagliero, J.A. Reimer, D. Suter, C.A. Meriles, A. Pines, “Orientation-independent room-temperature optical ¹³C hyperpolarization in powdered diamond”, *Science Adv.* **4**, eaar5492 (2018).

²⁰ P.R. Zangara, S. Dhomkar, A. Ajoy, K. Liu, R. Nazarian, D. Pagliero, D. Suter, J.A. Reimer, A. Pines, C.A. Meriles, “Dynamics of frequency-swept nuclear spin optical pumping in powdered diamond at low magnetic fields”, *Proc. Natl. Acad. Sci. USA* **116**, 2512 (2019).

²¹ See Supplementary Material for a derivation of the effective nuclear spin Hamiltonian and delocalization diagram, as well as a description of the electron/nuclear spin system response in the presence of RF.

²² A. De Luca, M. Collura, J. De Nardis, “Non-equilibrium spin transport in integrable spin chains: Persistent currents and emergence of magnetic domains”, *Phys. Rev. B* **96**, 020403 (2017).

- ²³ C.V. Peaker, M.K. Atumi, J.P. Goss, P.R. Briddon, A.B. Horsfall, M.J. Rayson, R. Jones, “Assignment of ^{13}C hyperfine interactions in the P1-center in diamond”, *Diam. Rel. Mater.* **70**, 118 (2016).
- ²⁴ K.R.K. Rao, D. Suter, “Characterization of hyperfine interaction between an NV electron spin and a first-shell ^{13}C nuclear spin in diamond”, *Phys. Rev. B* **94**, 060101(R) (2016).
- ²⁵ B. Smeltzer, L. Childress, A. Gali, “ ^{13}C hyperfine interactions in the nitrogen-vacancy centre in diamond”, *New J. Phys.* **13**, 025021 (2011).
- ²⁶ A. Dreau, J.R. Maze, M. Lesik, J-F. Roch, V. Jacques, “High-resolution spectroscopy of single NV defects coupled with nearby ^{13}C nuclear spins in diamond”, *Phys. Rev. B* **85**, 134107 (2012).
- ²⁷ J. Kimball, “Comments on the interplay between Anderson localization and electron-electron interactions”, *J. Phys. C: Solid State Phys.* **14**, L1061 (1981).
- ²⁸ G.A. Álvarez, D. Suter, R. Kaiser, “Localization-delocalization transition in the dynamics of dipolar-coupled nuclear spins”, *Science* **349**, 846, (2015).
- ²⁹ J. Choi, S. Choi, G. Kucsko, P.C. Maurer, B.J. Shields, H. Sumiya, S. Onoda, J. Isoya, E. Demler, F. Jelezko, N.Y. Yao, M.D. Lukin, “Depolarization dynamics in a strongly interacting solid-state spin ensemble”, *Phys. Rev. Lett.* **118**, 093601 (2017).
- ³⁰ K.X. Wei, C. Ramanathan, P. Cappellaro, “Exploring localization in nuclear spin chains”, *Phys. Rev. Lett.* **120**, 070501 (2018).
- ³¹ G. Kucsko, S. Choi, J. Choi, P.C. Maurer, H. Zhou, R. Landig, H. Sumiya, S. Onoda, J. Isoya, F. Jelezko, E. Demler, N.Y. Yao, M.D. Lukin, “Critical thermalization of a disordered dipolar spin system in diamond”, *Phys. Rev. Lett.* **121**, 023601 (2018).
- ³² P.R. Levstein, H.M. Pastawski, J.L. D’Amato, “Tuning the through-bond interaction in a two-centre problem”, *J. Phys.: Condens. Matter* **2**, 1781 (1990).
- ³³ J.R. Johansson, P.D. Nation, F. Nori, “QuTiP 2: A Python framework for the dynamics of open quantum systems”, *Comput. Phys. Commun.* **184**, 1234 (2013).